

## Photocatalytic Conversion of NO using TiO<sub>2</sub>-NH<sub>3</sub> Catalysts in Ambient Air Environment

F. B. Li<sup>1,2</sup>, X. Z. Li<sup>1\*</sup>, C.H. Ao<sup>1</sup>, M. F. Hou<sup>2</sup> and S.C. Lee<sup>1</sup>

<sup>1</sup>Department of Civil and Structural Engineering, The Hong Kong Polytechnic University,  
Hong Kong, China

<sup>2</sup>Guangdong Key Laboratory of Agricultural Environment Pollution Integrated Control, Guangdong Institute  
of Eco-Environmental and Soil Sciences, Guangzhou, 510650, China

**Abstract:** Photocatalytic conversion of nitric oxide (NO) in ambient air was studied in a continuous-flow photoreactor system at room temperature using different TiO<sub>2</sub> catalysts prepared with different titanium precursors of Ti(SO<sub>4</sub>)<sub>2</sub>, TiOSO<sub>4</sub>, and Ti(O-Bu)<sub>4</sub> by either a moderate-temperature hydrothermal process or a hydrothermal reflux process. The physicochemical properties of the prepared catalysts were characterized by XRD, BET, FTIR, and SEM. Analytical results showed that the crystallinity, morphology, nitrogen adsorption–desorption isotherms, specific surface area, and pore size distribution of catalysts were significantly affected by the precursors and hydrothermal processes, but the crystal structure and crystal size of catalysts were not significantly influenced. The NO conversion experiments demonstrated that the TiO<sub>2</sub> catalysts prepared by the moderate-temperature hydrothermal process without ammonia pretreatment could effectively reduce NO to different low levels, in which the catalysts with longer aging time of more than 12 h performed better than the catalysts with shorter aging time. However, it was found that the NO<sub>2</sub> concentration in outlet gas was gradually increased with extension of an experimental period. Two TiO<sub>2</sub> catalysts (TOSO-NH<sub>3</sub> and TOB-NH<sub>3</sub>) prepared by the hydrothermal reflux process with ammonia pretreatment demonstrated a very good performance in NO conversion and also maintained a low level of NO<sub>2</sub> concentration in outlet gas. This study indicated that using the TiO<sub>2</sub> catalysts modified with ammonia pretreatment in photocatalytic reaction could provide a good approach to effectively eliminate the accumulation of NO<sub>2</sub> product from NO oxidation in the system and to achieve a sustainable process, which may be applicable for NO elimination in ambient air environment.

**Keywords:** hydrothermal method; NO; photocatalysis; TiO<sub>2</sub>

---

\* Corresponding author: phone: (852) 2766 6016; Fax: (852) 2334 6389; Email: cexzli@polyu.edu.hk

## 1. Introduction

Nitrogen oxides ( $\text{NO}_x$ ) such as nitric oxide (NO), nitrous oxide ( $\text{N}_2\text{O}$ ), and nitrogen dioxide ( $\text{NO}_2$ ) exhausted from internal combustion engines and furnaces is a kind of harmful atmospheric pollutants which can cause acid rain, photochemical smog, and greenhouse effects. The content of nitric oxide (NO) in  $\text{NO}_x$  is usually more than 95% from exhaust gases and the rest is nitrogen dioxide ( $\text{NO}_2$ ). Either indoor or outdoor concentration of  $\text{NO}_x$  in many cities of China now exists the tolerable levels of the health and environmental criteria [1-2]. For example, the concentration of  $\text{NO}_x$  with a ratio of  $\text{NO}_2/\text{NO}_x = 0.86$  was found in Lanzhou Valley of China to be up to 54.0 and 71.2 ppb during the winters of 1999 and 2001, respectively. It was also found that the concentrations of NO and  $\text{NO}_2$  in some streets in Guangzhou of China was up to 128 and 112 ppb, respectively. In Hong Kong, a previous survey found that the concentration of NO in several markets varied from 39.2 to 58.4 ppb, while that of  $\text{NO}_2$  varied from 97.6 to 105.6 ppb [3].

To abate the  $\text{NO}_x$  emission, various de- $\text{NO}_x$  technologies have been developed with recent improvements [4-12]. Selective catalytic reduction (SCR) processes were applied at some stationary emission sources such as power plants, waste incinerators, and industrial boilers to transfer  $\text{NO}_x$  into  $\text{N}_2$  and  $\text{H}_2\text{O}$  at high temperature [4-8]. Furthermore, with appropriate catalysts and reducing agents such as ammonia ( $\text{NH}_3$ -SCR) or hydrocarbons (HC-SCR), the non-thermal plasma processes could be feasible to reduce nitric oxides synergistically into  $\text{N}_2$  [7]. It has been reported recently that some  $\text{NH}_3$ -SCR processes using either Rb-VS or  $\text{TiO}_2$  catalyst can successfully convert NO into  $\text{N}_2$  in the presence of  $\text{O}_2$  under LIGHT irradiation at even room temperature [9-12].

However, these  $\text{NH}_3$ -SCR processes may not be suitable for reduction of  $\text{NO}_x$  from ambient environment (either indoor or outdoor air) where ammonia is not available. Photocatalytic technology using solar energy for  $\text{NO}_x$  removal from ambient environment may have an attractive potential for application in practice. Hashimoto's group [13, 14], Matsuda's group [15], Tanaka's group [16], Dalton et al. [17], and Ichiura et al. [18] reported that NO can be transferred into  $\text{NO}_2$  and then into nitric acid ( $\text{HNO}_3$ ) in a  $\text{TiO}_2$ -based photocatalytic oxidation system. In reality, the formation of  $\text{NO}_2$  and  $\text{HNO}_3$  need to be minimized, since they are harmful to environment. Anpo's group [19-25] reported that  $\text{NO}_x$  could be directly decomposed into  $\text{N}_2$ ,  $\text{N}_2\text{O}$ , and  $\text{O}_2$  by using photocatalysts including vanadium silicalite (VS-2), Ti-HMS, V oxide/ZSM-5,  $\text{Ag}^+$ -doped ZSM-5

zeolites, TiO<sub>2</sub>/ZSM-5, or pure TiO<sub>2</sub> powder under illumination from a high-pressure Hg lamp or a Xenon lamp at different temperature, even at room temperature. For example, NO was selectively decomposed into N<sub>2</sub> by 27% and N<sub>2</sub>O by 73% at 275 K using TiO<sub>2</sub> powder (Degussa P-25) and more N<sub>2</sub> was formed when Ti/Y or Ti/ZSM-5 catalyst was used under a mixed flow of 20 cm<sup>3</sup> min<sup>-1</sup> O<sub>2</sub> gas and 20 cm<sup>3</sup> min<sup>-1</sup> Ar gas [24]. Obviously, the requirement of Ar gas in these processes is a difficulty for its real application in practice. Moreover, Yomashita's group reported NO could be transferred into N<sub>2</sub>O with a small amount of N<sub>2</sub> and NO<sub>2</sub> at 310 K in the presence of 10% O<sub>2</sub> in N<sub>2</sub> balance under Xe lamp irradiation in a continuous-flow reactor over AgCl/Al<sub>2</sub>O<sub>3</sub> catalyst [25]. These results indicated that the photocatalytic oxidation of NO to NO<sub>2</sub> and reduction of NO to N<sub>2</sub> could occur in the presence of O<sub>2</sub> and N<sub>2</sub> simultaneously. In fact, the air is mainly composed of 20% O<sub>2</sub> and 80% N<sub>2</sub>, which may be possible to provide a suitable environment to conduct the both reactions in a photoreactor system. However, the above-mentioned photocatalysts except TiO<sub>2</sub> are all unfriendly to environment and can not be used for NO<sub>x</sub> control in outdoor or indoor air environment. Therefore, it should be meaningful to investigate TiO<sub>2</sub>-based photocatalytic reaction for NO conversion at ambient temperature, because TiO<sub>2</sub> is a non-toxic and environmentally friendly photocatalyst. However, a controversial point is that the activity using TiO<sub>2</sub> to remove NO is generally low and NO can only be partially converted into NO<sub>2</sub> and then HNO<sub>3</sub> in the presence of O<sub>2</sub>. Therefore, it is necessary to seek for more effective ways to depress the formation of NO<sub>2</sub> and HNO<sub>3</sub> and to obtain a higher efficiency of NO reduction simultaneously. In general, large surface area and good crystallinity of catalysts are beneficial to the TiO<sub>2</sub>-based photocatalysis in an air phase. Hydrothermal processes can be applied to synthesize the TiO<sub>2</sub>-based catalysts with high surface area and crystallinity. [27-34]

In this study, several TiO<sub>2</sub>-based catalysts were prepared by either a moderate-temperature hydrothermal process [27-30] or a hydrothermal reflux process [31-34]. NO conversion was evaluated in the presence of air under LIGHT irradiation and the effect of hydrothermal processes on the NO conversion efficiency was investigated. The physicochemical properties of the prepared TiO<sub>2</sub> catalysts were fully characterized and a relationship between physicochemical properties and NO conversion efficiency was discussed.

## 2. Experimental Section

## 2.1 Preparation of TiO<sub>2</sub> catalysts

A series of TiO<sub>2</sub> catalysts using Ti(SO<sub>4</sub>)<sub>2</sub> as a titanium precursor was prepared by a hydrothermal method [27-30] at moderate temperature with the following procedure: Ti(SO<sub>4</sub>)<sub>2</sub> was first mixed with distilled water to prepare a mixture with a concentration of 0.6 mol l<sup>-1</sup>; Then the mixture was stirred for 10 min and aged in a PTFE-lined autoclave at 393 K for different time from 6 to 24 h; After quenching the autoclave in the cold water, the precipitated powder was collected, washed with distilled water for 5 times to remove sulfate ion, filtered, and finally dried at 378 K for 24 h. The product TiO<sub>2</sub> samples with different time of 6, 9, 12, 16, and 20 h were named TSO-6, TSO-9, TSO-12, TSO-16, and TSO-20, respectively.

A TiO<sub>2</sub> catalyst using TiOSO<sub>4</sub> as a precursor was prepared by a hydrothermal method [27-30] with the following procedure: TiOSO<sub>4</sub> chemical was mixed with distilled water to prepare a mixture with a concentration of 0.6 mol l<sup>-1</sup>; Then the mixture was stirred for 10 min and aged at 393 K for 12 h in a PTFE-lined autoclave; After quenching the autoclave in the cold water, the precipitated powder was collected, washed with distilled water for 5 times, filtered, and finally dried at 378 K for 24 hours. This TiO<sub>2</sub> sample was named TOSO-12.

A TiO<sub>2</sub> catalyst using Ti(O-Bu)<sub>4</sub> as a precursor was prepared by a hydrothermal reflux method [31-34] with the following procedure: 17.28 ml of Ti(OC<sub>4</sub>H<sub>9</sub>)<sub>4</sub> was dissolved in 115 ml of absolute ethanol to obtain a sol mixture; Then 20 ml of 2 mol l<sup>-1</sup> NH<sub>3</sub>•H<sub>2</sub>O solution was added dropwise into the sol mixture under vigorous stirring at room temperature; The resulting suspension was stirred for 0.5 h; The precipitated powder was centrifuged and washed four times with distilled water; Then the collected powder was added into 200 ml of 0.05 mol l<sup>-1</sup> HNO<sub>3</sub> solution, and the suspension was refluxed for 2 h at 353 K, and then centrifuged; The TiO<sub>2</sub> catalyst was finally obtained after washing with distilled water four times and dried for 24 h at 333 K. The product TiO<sub>2</sub> sample was named TOB-NH<sub>3</sub>.

A TiO<sub>2</sub> catalyst using TiOSO<sub>4</sub> as a precursor was prepared by the hydrothermal reflux method [31-34], in which 20 g of TiOSO<sub>4</sub> was dissolved into a mixture solution with 100 ml of absolute ethanol and 400 ml of distilled water. The mixture solution was refluxed at 353 K for 2 h. After filtered and washed four times, the collected powder was then washed with 1000 ml of 2 mol l<sup>-1</sup>

NH<sub>3</sub>•H<sub>2</sub>O solution and was dried at 373 K for 24 h. The product TiO<sub>2</sub> sample was named TOSO-NH<sub>3</sub>.

## 2.2 Characterization of TiO<sub>2</sub> catalysts

To determine the crystal phase composition of the TiO<sub>2</sub> catalysts, X-ray diffraction (XRD) measurement was carried out at room temperature using a Rigaku D/MAX-III A diffractometer with CuK<sub>α</sub> radiation ( $\lambda = 0.15418$  nm). The accelerating voltage of 35 kV and emission current of 30 mA were applied. The specific surface area, t-plot total surface area, t-plot surface area, monolayer volume, micropore surface area, and total pore volume of all samples were measured by the Brunauer-Emmett-Teller (BET) method, in which the N<sub>2</sub> adsorption at 77 K using a Carlo Erba Sorptometer was applied. The pore-size distribution of the catalysts was determined by the Barrett-Joyner-Halenda (BJH) method. The surface morphology of the catalysts was observed using scanning electron microscopy (SEM Leica Stereoscan 400i series). Fourier transform infrared spectra of the catalysts were also recorded with a FT-IR spectrometer (Perkin-Elmer) at room temperature.

## 2.3 Materials

NO gas from a compressed gas cylinder with nitrogen balance was used in this study for NO reduction experiments, which was supplied by BOC Gases with a concentration of 50 ppmv  $\pm$  2% with the traceable NIST standard (National Institute of Standards and Technology). The prepared TiO<sub>2</sub> catalysts were diffused into distilled water to make 5% (w/w) suspension. Then the TiO<sub>2</sub> suspension was gradually dropped and the catalyst was coated on a glass fiber filter (Whatman) as a supporting medium over an area of 20 cm  $\times$  21 cm. This TiO<sub>2</sub>-coated filter was then calcinated at 370 K for 1 h with a temperature gradient at 5.5 K per min from room temperature. The amount of TiO<sub>2</sub> imposed was determined by weighing the difference before and after the coating. In all experiments, the weight of TiO<sub>2</sub> coated was determined to be 1.64 g  $\pm$  5%.

## 2.4 Experimental Setup

A photoreactor with an effective volume of 18.6 liter (20.1 H  $\times$  44.2 L  $\times$  21 W cm) was used for this study, which surface was coated with a Teflon film (BYTAC Type AF-21). Illumination was provided by a 6W UV lamp (Cole-Parmler) with a main emission at the wavelength of 365 nm. The

UV lamp was horizontally placed at the upper-middle part of the photoreactor about 14 cm away from both sides. The TiO<sub>2</sub>-coated filter was horizontally sited at the lower part of the photoreactor with a vertical distance of 5 cm from the UV lamp. The light intensity on the TiO<sub>2</sub> surface was determined to be 750 μW cm<sup>-2</sup> by a UV radiator (Spectroline DRC-100X). Stainless-steel sampling ports and Teflon tubing were used to connect the photoreactor and the analytical instruments.

A Zero air generator (Thermo Environmental Inc. Model 111) was used to supply an air stream. The desired humidity of the flow was controlled by passing the Zero air stream through a humidification chamber. A reactant gas stream from the NO gas cylinder was premixed with the Zero air stream by a gas blender, in which both gas flows were regulated by two mass flow controllers inside a mass flow calibrator (Advanced Pollution Instrumentation Inc. Model 700). Then the mixed gas stream containing an initial NO concentration of 200 ppb ± 2% as inflow was introduced to the photoreactor. When the NO concentrations of inlet and outlet have reached an equilibrium condition after about 1 h, the UV lamp was turned on to start the reaction. A gas inflow rate was maintained at 15 l min<sup>-1</sup> and the photocatalytic reaction was conducted at temperature of 298 K under a pressure of about 1 atm within the photoreactor. During the reaction, the NO concentrations at inlet and outlet were continuously monitored and NO conversion was evaluated according to the definition of NO conversion =  $\frac{[NO]_{inlet} - [NO+NO_2]_{outlet}}{[NO]_{inlet}} \times 100\%$ .

## 2.5 Analyses

The concentrations of NO, NO<sub>2</sub>, and NO<sub>x</sub> were measured by a Chemiluminescence NO<sub>x</sub> analyzer (Thermo Environmental Instruments Inc. Model 42c) at a sampling rate of 0.7 l min<sup>-1</sup>.

## 3. Results and Discussion

### 3.1 Crystal Structure and Size of TiO<sub>2</sub> Catalysts

The XRD photographs of the TSO-X catalysts prepared with Ti(SO<sub>4</sub>)<sub>2</sub> as precursor at different hydrothermal time are presented in Fig. 1A and showed an anatase structure. The crystal size of these catalysts was determined by the Scherrer equation to be between 18.0-19.8 nm as listed in Table 1. These results indicated that the hydrothermal time seems not significant to influence the crystal size. On the other hand, the XRD results indicated that the crystallinity of the TSO-X

catalysts was improved with the extension of hydrothermal time, but more significantly from 6 to 9 h than from 12 to 20 h as shown in Fig. 1A. The XRD photographs of the TiO<sub>2</sub> catalysts prepared with other precursors are presented in Fig. 1B and also demonstrated a well-developed anatase structure. The crystal size of the catalysts as listed in Table 2 was between 17.1-21.0 nm. These results further confirmed that either the precursors or hydrothermal processes did not affect the crystal size significantly. However, it was found that the crystallinity of TiO<sub>2</sub> samples prepared by the hydrothermal reflux method was much poorer than that by the moderate-temperature hydrothermal process as shown in Fig. 1B.

### **3.2 Surface Area, Pore Size, and Morphology of TiO<sub>2</sub> Catalysts**

The specific surface area, t-plot total surface area, t-plot surface area, monolayer volume, porous surface area, and total pore volume of TiO<sub>2</sub> samples were measured by the BET method. The analytical results for the TSO-X catalysts prepared at different hydrothermal time are listed in Table 1 and the results for the other catalysts prepared in different processes are presented in Table 2. The BET data in Table 1 showed that BET surface area, t-plot surface area, and total pore volume increased with the hydrothermal time from 6 to 12 h and then decreased with the longer hydrothermal time from 12 to 20 h. The data in Table 2 indicated that TOSO-NH<sub>3</sub> sample had the largest t-plot total surface area and TOB-NH<sub>3</sub> sample had no micropore volume at all. It is obvious that the TiO<sub>2</sub> samples prepared by the hydrothermal reflux process had much smaller micropore volume and total pore volume than those by the moderate-temperature hydrothermal process.

To investigate the effects of different titanium precursors, hydrothermal processes, and hydrothermal treatment time on the pore structure and adsorption property of TiO<sub>2</sub> samples, a set of nitrogen adsorption/desorption tests was carried out and their isotherms are presented in Figs. 2A and 2B. It can be seen from Fig. 2A that the isotherms of the TSO-X catalysts showed a typical shape of Type IV curves [35] and their narrow hysteresis loops exhibited a typical pattern of Type H3 at a relative pressure from about 0.44 to 1. The isotherms of other catalysts as shown in Fig. 2B demonstrated that TOSO-12 had a narrow hysteresis loop of Type H3 and exhibited at relative pressure from about 0.44 to 1, while TOB-NH<sub>3</sub> and TOSO-NH<sub>3</sub> had a hysteresis loop of Type II and exhibited at relative pressure from about 0.4 to 0.8. The above results indicated that these catalysts might have a porous structure. The analytical results of pore-size distribution are shown in Figs. 3A

and 3B. The results in Fig. 3A showed that the TSO-X catalysts prepared by the hydrothermal process at 397 K had mainly a disordered-mesoporous structure and their pore volume varied against the pore size in the main range of 4-55 nm with a maximum portion at about 16 nm. This mesoporous structure was attributed to the pores formed between TiO<sub>2</sub> particles [36-38]. Furthermore, the pore-size distribution as shown in Fig. 3B demonstrated that the different catalysts had different pore structures. TOSO-NH<sub>3</sub> showed a significant microstructure with much lower average pore size between 2-5 nm. TOB-NH<sub>3</sub> demonstrated a mixture of microporous structure with a negligible micropore volume and mesoporous structure with the maximum pore size located at about 3.65 nm. TOSO-12 showed a mixture of mesoporous and macroporous structures with a diffusive porosity in the range of 4-100 nm and a maximum portion at about 22 nm. The morphology of the different catalysts was examined by SEM, as shown in Fig. 4. The mixture of mesoporous and macroporous structures formed on the TiO<sub>2</sub> catalysts of TSO-12 and TOSO-12 can be clearly seen in Figs. 4A and 4B, respectively, compared to the catalysts of TOB-NH<sub>3</sub> and TOSO-NH<sub>3</sub> shown in Figs. 4C and 4D, respectively. These SEM results were well matched with the BET results.

[FIG. 2]

[FIG. 3]

[FIG. 4]

### 3.3 FTIR Analyses

The FTIR spectra of the prepared TiO<sub>2</sub> catalysts are presented in Fig. 5. For all samples, the broad peak at 3400-3700 cm<sup>-1</sup> and the strong peak at 1,636 cm<sup>-1</sup> are attributed to O-H stretching vibration of water and OH group on the TiO<sub>2</sub> surface. For TSO-6, TSO-9, TSO-12, and TSO-20, the four peaks at 901, 980, 1,055, and 1,132 cm<sup>-1</sup> could be assigned to the stretching vibration of the sulfate ion chemisorbed on the surface and the sulfate ion could be suggested to bond to the surface Ti<sup>4+</sup> ion to form some surface complexes such as TiO<sub>2</sub>-SO<sub>4</sub><sup>2-</sup>. For TOB-NH<sub>3</sub> and TOSO-NH<sub>3</sub>, the peak at 1400 cm<sup>-1</sup> might be attributed to the NH<sub>3</sub> adsorbed on Lewis acid site of TiO<sub>2</sub> and all the peaks attributable to sulfate ion disappeared almost completely. This means that the adsorbed sulfate ion could be more easily removed by washing with aqueous ammonia. Moreover, the peaks attributable



to the chemisorbed sulfate ion and adsorbed  $\text{NH}_3$  disappeared almost for TOSO-12.

[FIG. 5]

### 3.4 NO Conversion

A set of experiments to remove NO from a gaseous phase was carried out in the continuous flow reactor system using different catalysts. The NO gas stream with an initial concentration of  $200 \pm 5\%$  ppb in air and a humidity level of 15,700 ppm passed through the reactor at a flow rate of  $15.5 \text{ l min}^{-1}$  with an empty bed retention time (EBRT) of 72 s. After a stabilized period of about one hour, NO concentration in outlet gas became as same as that in inlet gas and the experiment commenced by simply turning on the UV lamp. The concentrations of NO and  $\text{NO}_2$  were recorded by the  $\text{NO}_x$  analyzer at every one minute. The experimental results of NO and  $\text{NO}_2$  concentrations against the reaction time are shown in Figs. 6A and 6B, respectively. Obviously, the concentration of NO dropped rapidly and reached a steady-state concentration after 5 min. For the catalysts of TSO-12, TSO-16, and TSO-20, the steady-state concentration were kept unchanged at 34.4, 36.3, and 37.3 ppb, respectively during the experiment, while the steady-state concentration significantly increased with the reaction time for the catalysts of TSO-6 and TSO-9. In the meantime, the amount of  $\text{NO}_2$  generated increased obviously with the reaction time and there was no steady-state concentration found within 120 min for all TSO-X catalysts. In fact,  $\text{NO}_2$  was formed continuously and further transferred into  $\text{HNO}_3$  during the irradiation time. When an excess amount of  $\text{HNO}_3$  was adsorbed on the catalyst surface, the photoactivity would decrease. The increase of NO and  $\text{NO}_2$  concentrations indicated deactivation of photocatalyst during NO photodegradation. The conversion of  $\text{NO}_x$  for the catalysts of TSO-6, TSO-9, TSO-12, TSO-16, and TSO-20 was found to be 33.5%, 44.1%, 65.9%, 65.8%, and 64.2%, respectively as shown in Fig. 7. In fact, the difference of NO conversion for TSO-12, TSO-16, and TSO-20 was found to be less compared to that for TSO-6 and TSO-9. It is generally believed that the photocatalytic activity of  $\text{TiO}_2$  catalysts depends on the crystal size, crystallinity, specific surface area, pore volume, pore-size distribution, and surface state. For the above 5 catalysts, TSO-6 and TSO-9 had poor crystallinity and small surface area, therefore their activity for NO conversion was lower than TSO-12. TSO-12 had a higher specific surface area and then had a higher activity for NO conversion than TSO-16 and TSO-20.

[FIG. 6]

[FIG. 7]

Under the same conditions, NO in a gas flow was also decomposed using other catalysts of TSO-12, TOSO-12, TOB-NH<sub>3</sub>, TOSO-NH<sub>3</sub>, and P-25. The variations of NO and NO<sub>2</sub> concentrations in outlet gas are shown in Figs. 8A and 8B. It can be seen that the NO concentration dropped rapidly and then reached a steady-state concentration. For the catalysts of TSO-12, TOSO-12, TOB-NH<sub>3</sub>, and TOSO-NH<sub>3</sub>, the steady-state concentration occurred quickly within 3 min and was kept unchanged at 34.4, 33.9, 30.2, and 30.5 ppbv, respectively until the experiment was complete, while for the catalyst of P-25, the steady-state concentration occurred much later at around 60 min and was kept unchanged at 36.7 ppbv. In the meantime, the NO<sub>2</sub> concentration increased quickly in the first 10 min and gradually reached their steady-state concentrations of 20.9 ppb at 40 min for the catalyst of TOB-NH<sub>3</sub> and 15.7 ppbv at 60 min for the catalyst of TOSO-NH<sub>3</sub>, respectively. The NO<sub>2</sub> concentration for the catalysts of TSO-12, TOSO-12 and P25 continuously increased throughout the whole reaction time. During the photoreaction, NO<sub>2</sub> was continuously formed and eventually transferred into HNO<sub>3</sub> in this photocatalytic oxidation environment. When an excess amount of HNO<sub>3</sub> was adsorbed on the surface of P-25, TOSO-12, and TSO-12, nitrate ion might occupy the reaction site and then the photocatalytic efficiency for NO conversion decreased with reaction time. It has been determined that the conversion percentage of NO in 120 min for TOSO-12, TOB-NH<sub>3</sub>, TOSO-NH<sub>3</sub> and P-25 was 63.0%, 75.4%, 76.6%, and 69.5%, respectively as shown in Fig. 7. It is clear that TOSO-NH<sub>3</sub> had the highest photoactivity for NO conversion and was more active than P-25. The activity of TOB-NH<sub>3</sub> was slightly lower than that of TOSO-NH<sub>3</sub> because its specific surface area was much less than that of TOSO-NH<sub>3</sub>.

[FIG. 8]

In the present reaction system, when NO in air entered the reactor, a homogeneous reaction of  $\text{NO} + \frac{1}{2}\text{O}_2 \rightarrow \text{NO}_2$  ( $\Delta G^0 = -8.89 \text{ kcal mol}^{-1}$ ) could occur to convert NO into NO<sub>2</sub> directly under irradiation. In the meantime, TiO<sub>2</sub> catalyst was excited under LIGHT illumination to form hydroxyl radical and NO was also transferred into NO<sub>2</sub> and then HNO<sub>3</sub> by this photocatalytic oxidation reaction. However, nitrate ions would be adsorbed on the Lewis-acid site of TiO<sub>2</sub> surface and gradually these

nitrate ions occupied the most Lewis-acid site. This competitive adsorption between nitrate ion and NO decreased the rate of photocatalytic oxidation from NO to NO<sub>2</sub> on the catalyst surface and encouraged the direct oxidation from NO to NO<sub>2</sub> in the gaseous phase. Therefore, the conversion percentage of NO for TSO-6, TSO-9, TSO-12, TSO-16, TSO-20, and TOSO-12 decreased against reaction time and the NO<sub>2</sub> concentration increased with reaction time continuously. The above 6 catalysts demonstrated this weakness significantly. However, both the TOSO-NH<sub>3</sub> and TOB-NH<sub>3</sub> catalysts demonstrated a different behavior. The NO<sub>2</sub> concentration in outlet gas was maintained at a very low level. According to the proposal by Teramura et al. [12], when NH<sub>3</sub> is adsorbed on the Lewis acid site (Ti-O-Ti) of TiO<sub>2</sub> catalysts, both of Ti-NH<sub>2</sub> (radical amide) and Ti-OH are formed under LIGHT irradiation. Under this condition, NO can attack Ti-NH<sub>2</sub> on the TiO<sub>2</sub> catalysts in the presence of O<sub>2</sub> and form N<sub>2</sub> (NO + NH<sub>3</sub> + O<sub>2</sub> → N<sub>2</sub> + H<sub>2</sub>O). In the meantime, NO can also be directly adsorbed on the Lewis acid site of TiO<sub>2</sub> catalysts unoccupied by NH<sub>3</sub> and oxidized into NO<sub>2</sub> under LIGHT irradiation. The product NO<sub>2</sub> is partially further oxidized to HNO<sub>3</sub> and is also be partially reduced into N<sub>2</sub> (NO<sub>2</sub> + NH<sub>3</sub> → N<sub>2</sub> + (3/2) H<sub>2</sub>O + (1/4) O<sub>2</sub>), because free energy of the reaction at room temperature is negative. In fact, Tanaka et al. [16] reported that photo-assisted SCR of NO with ammonia could happen in the presence of O<sub>2</sub> and Ar under room temperature and atmospheric pressure and could not happen in the absence of ammonia for TiO<sub>2</sub>/SiO<sub>2</sub> photocatalysts. Jung and Grange [39] reported the SCR of NO with ammonia in the presence of O<sub>2</sub> could be activated at 450°C without irradiation. Therefore, for TOSO-NH<sub>3</sub> and TOB-NH<sub>3</sub>, the photoactivity for NO conversion could keep stable owing to the presence of ammonia adsorbed in the Lewis acid site of TiO<sub>2</sub> catalysts. By the way, during this reduction reaction, NH<sub>3</sub> acts as a reactant and TiO<sub>2</sub> acts as a catalyst. The mass of NH<sub>3</sub> on the surface of TiO<sub>2</sub> catalyst would gradually decrease during the reaction. Therefore, to maintain a high reaction rate of NO<sub>x</sub> conversion, the exhaust catalysts need to be retreated with the addition of NH<sub>3</sub> periodically. Unfortunately, the formation of N<sub>2</sub> could not be tested due to the limits of experimental conditions in this study. However, the higher efficiency of NO conversion and a lower formation of NO<sub>2</sub> had been obtained by using TiO<sub>2</sub> catalysts prepared by hydrothermal reflux process with ammonia pretreatment. Further clarification of the reaction mechanism is now under progress. On the other hand, TiO<sub>2</sub> photo-assisted NO removal process can be used for indoor air purification and this technology is more meaningful to outdoor air purification on a large scale because solar spectrum can be used a light source [40, 41] and TiO<sub>2</sub> can be coated on the outer wall of any building or trees on the side of streets or any other support.

## Conclusions

Photocatalytic conversion of NO in ambient air environment was investigated using several types of TiO<sub>2</sub> catalysts in this study. It was found that NO could be effectively converted into NO<sub>2</sub> and then HNO<sub>3</sub>. However, experiments demonstrated that the accumulated nitrate ions on the catalyst surface would result in a lower photoactivity of the TiO<sub>2</sub> catalysts without ammonia pretreatment. Alternatively, the ammonia-pretreated TiO<sub>2</sub> catalysts of TOSO-NH<sub>3</sub> and TOB-NH<sub>3</sub> could effectively consume the further product of NO<sub>2</sub> to maintain both the concentrations of NO and NO<sub>2</sub> at very low levels throughout the whole experimental time, since both the photocatalytic oxidation from NO to NO<sub>2</sub> and reduction from NO<sub>2</sub> to N<sub>2</sub> were taken simultaneously in this photoreactor system. This study indicated that photocatalytic conversion of NO in air using the ammonia-treated TiO<sub>2</sub> catalysts would provide a good approach to eliminate NO concentration in ambient air environment to a very low level.

## Acknowledgement

The authors wish to thank the Hong Kong Polytechnic University for a financial support to this work under a Postdoctoral Fellowship Grant (Project No.: G-YW69/02) and National Natural Science Foundation Project No. 20203007.

## References

1. S. D. Xie, Y. H. Zhang, X. Y. Tang, *Atmospheric Environment*, 37 (2003) 3213.
2. W. Q. Ta, T. Wang, H. L. Xiao, X. Y. Zhu, Z. Xiao, *Sci. Total Environ.* 2003, in pressing.
3. H. Guo, S. C. Lee, L. Y. Chan, *Sci. Total Environ.* 2003, in pressing.
4. Y. S. Mok, D. J. Koh, K. T. Kim, I. S. Nam, *Ind. Eng. Chem. Res.* 42 (2003) 2960.
5. R. Q. Long, R. T. Yang, *J. Catal.* 207 (2002) 158.
6. M. A. Centeno, P. Malet, I. Carrizosa, J. A. Odriozola, *J. Phys. Chem. B* 104 (2000) 3310.
7. H. Miessner, K.-P. Francke, R. Rudolph, T. Hammer, *Catal. Today.* 75 (2002) 325.
8. J. H. Choy, H. Jung, Y. S. Han, J. B. Yoon, Y. G. Shul, H. J. Kim, *Chem. Mater.* 14 (2002) 3823.
9. G. Madia, M. Koebel, M. Elsener, A. Wokaun, *Ind. Eng. Chem. Res.* 41 (2002) 3512.
10. F. Notoya, E. Sasaoka, S. Nojima, *Ind. Eng. Chem. Res.* 40 (2001) 3732.
11. T. Tanaka, K. Teramura, T. Funabiki, *Phys. Chem. Chem. Phys.* 2 (2000) 2681.

12. K. Teramura, T. Tanaka, T. Funabiki, *Langmuir*. 19 (2003) 1209.
13. K. Hashimoto, K. Wasato, N. Toukai, H. Kominami, Y. Kera, *J. Photochem. Photobiol. A Chem.* 136 (2000) 103.
14. K. Hashimoto, K. Wasato, M. Osaki, E. Shono, K. Adachi, N. Toukai, H. Kominami, Y. Kera, *Appl. Catal. B* 30 (2001) 429.
15. S. Matsuda, H. Hatano, A. Tsutsumi, *Chem. Engin. J.* 82 (2001) 183.
16. T. Tanaka, K. Teramura, T. Yamamoto, S. Takenaka, S. Yoshida, T. Funabiki, *J. Photochem. Photobiol. A Chem.* 148 (2002) 277.
17. J. S. Dalton, P. A. Janes, N. G. Jones, J. A. Nicholson, K. R. Hallam, G. C. Allen, *Environ. Pollution*. 120 (2002) 415.
18. H. Ichiura, T. Kitaoka, H. Tanaka, *Chemosphere*. 51 (2003) 855.
19. M. Anpo, S. G. Zhang, S. Higashimoto, M. Matsuoka, H. Yamashita, *J. Phys. Chem. B* 103 (1999) 9295.
20. J. L. Zhang, M. Minagawa, T. Ayusawa, S. Natarajan, H. Yamashita, M. Matsuoka, M. Anpo, *J. Phys. Chem. B* 104 (2000) 11501.
21. S. Higashimoto, M. Matsuoka, H. Yamashita, M. Anpo, O. Kitao, H. Hidaka, M. Che, E. Giamello, *J. Phys. Chem. B* 104 (2000) 10288.
22. S. M. Kanan, M. A. Omary, H. H. Patterson, M. Matsuoka, M. Anpo, *J. Phys. Chem. B* 104 (2000) 3507.
23. J. L. Zhang, T. Ayusawa, M. Minagawa, K. Kinugawa, H. Yamashita, M. Matsuoka, Anpo M. *J. Catal.* 198 (2001) 1.
24. J. L. Zhang, Y. Hu, M. Matsuoka, H. Yamashita, M. Minagawa, H. Hidaka, K. Kinugawa, M. Anpo, *J. Phys. Chem. B* 105 (2001) 8395.
25. C. H. Tseng, T. C. Keener, *Environ. Sci. Technol.* 35 (2001) 3219.
26. Y. Yamashita, N. Aoyama, N. Takezawa, Y. Kiyohide, *Environ. Sci. Technol.* 34 (2000) 5211.
27. Y. V. Kolen'ko, A. A. Burukhin, B. R. Churagulov, N. N. Oleynikov, *Materials Letters*, 57 (2003) 1124.
28. S. Yamabi, H. Imai, *Thin Solid Films* 434 (2003) 86.
29. M. Inagaki, Y. Nakazawa, M. Hirano, Y. Kobayashi, M. Toyoda, *International Journal of Inorganic Materials* 3 (2001) 809.
30. M. Andersson, L. Osterlund, S. Ljungstrom, A. Palmqvist, *J. Phys. Chem. B* 106 (2002) 10674.
31. R. T. Wu, Y. Wei, Y. F. Zhang, *Mater. Res. Bull.* 34 (1999) 2131.
32. V. A. Yasir, P. N. MohanDas, K. K. M. Yusuff, *International Journal of Inorganic Materials* 3 (2001)

33. M. Iwasaki, M. Hara, S. Ito, *J. Mater. Sci. Lett.* 17 (1998) 1769.
34. S. Ito, S. Inoue, H. Kawada, M. Hara, M. Iwasaki, H. Tada, *J. Coll. Interface. Sci.* 216 (1999) 59.
35. S. L. Gregg, K. S. W. Sing, *Adsorption, Surface Area and Porosity*, Academic Press, London, 1982.
36. J. G. Yu, J. C. Yu, M. K.-P. Leung, W. K. Ho, B. Cheng, X. J. Zhao, J. C. Zhao, *J. Catal.* 217 (2003) 69.
37. J. G. Yu, J. C. Yu, B. Cheng, S. K. Hark, K. Iu, *J. Solid State Chem.*, 174 (2003) 372.
38. J. C. Yu, J. G. Yu, W. K. Ho, L. Z. Zhang, *Chem. Commun.*, (2001) 1942.
39. S. M. Jung, P. Grange, *Appl. Catal. A: Gen.* 228 (2002) 65.
40. M. Anpo, Y. Ichihashi, M. Takeuchi, H. Yamashita, *Res. Chem. Intermed.*, 24 (1998) 143.
41. M. Anpo, Y. Ichihashi, H. Yamashita, Y. Tamada, P. Heide, R. R. Martin and T. Yoshinari, *Optronics*, 186 (1998) 161.

Table 1. Crystal size and BET data of TSO-X catalysts with different hydrothermal time

Catalyst	TSO-6	TSO-9	TSO-12	TSO-16	TSO-20
Crystal size (nm)	18.8	18.8	18.8	18.0	19.8
BET surface area ( $\text{m}^2 \text{g}^{-1}$ )	145.76	154.07	163.14	143.99	133.35
Monolayer pore volume ( $\text{cm}^3 \text{g}^{-1}$ , STP)	33.48	35.39	37.47	33.07	30.63
One point BET surface area ( $\text{m}^2/\text{g}$ ) ( $P_s/P_0 = 0.3$ )	144.94	153.13	162.21	143.03	132.50
t-plot surface area ( $\text{m}^2 \text{g}^{-1}$ )	138.22	155.89	158.87	149.32	140.54
t-plot total surface area ( $\text{m}^2 \text{g}^{-1}$ )	157.63	169.63	177.95	159.11	148.65
Micropore surface area ( $\text{m}^2 \text{g}^{-1}$ )	19.41	13.74	9.79	19.09	8.12
Micropore volume ( $10^{-3} \text{cm}^3 \text{g}^{-1}$ )	8.05	4.97	3.07	7.46	2.36
Total pore volume ( $\text{cm}^3 \text{g}^{-1}$ ) ( $P_s/P_0=0.9814$ , adsorption)	0.248	0.313	0.296	0.263	0.309

Table 2 Crystal size and BET data of different catalysts

Photocatalyst	TOSO-NH <sub>3</sub>	TOSO-12	TOB-NH <sub>3</sub>	TSO-12
Crystal size (nm)	17.1	21.0	21.0	15.3
BET surface area ( $\text{m}^2/\text{g}$ )	166.03	143.28	155.34	163.14
Monolayer volume ( $\text{cm}^3/\text{g}$ , STP)	38.14	32.91	35.68	37.47
One point BET surface area ( $\text{m}^2/\text{g}$ ) ( $P_s/P_0=0.3$ )	164.63	142.40	154.32	162.21
t-plot surface area ( $\text{m}^2/\text{g}$ )	200.59	137.66	171.14	158.87
t-plot total surface area ( $\text{m}^2/\text{g}$ )	222.20	154.88	175.57	177.95
Micropore surface area ( $\text{m}^2/\text{g}$ )	4.43	17.22	0.00	9.79
Micropore volume ( $10^{-3} \text{cm}^3/\text{g}$ )	1.30	6.75	0.000	3.07
Total pore volume ( $\text{cm}^3/\text{g}$ ) ( $P_s/P_0= 0.9814$ , adsorption)	0.157	0.380	0.196	0.296

FIG. 1. XRD photograph of TSO-X catalysts with different hydrothermal time (A) and other catalysts with the hydrothermal time of 12 h (B)

FIG. 2. Nitrogen adsorption-desorption isotherms of TSO-X catalysts with different hydrothermal time (A) and other catalysts with the hydrothermal time of 12 h (B)

FIG. 3. Pore-size distribution of TSO-X catalysts with different hydrothermal time (A) and other catalysts with the hydrothermal time of 12 h (B)

FIG. 4. The SEM photos of different catalysts

FIG. 5. FTIR spectra of different catalysts

FIG. 6. The dependence of NO concentration (A) and NO<sub>2</sub> concentration (B) on the reaction time under 6W Black lamp at humidity of 9400 ppmv with a retention time of 72 s by using TiO<sub>2</sub> powders prepared by hydrothermal process at different time.

FIG. 7. Photocatalytic conversion of NO in 120 min using different catalysts

FIG. 8. NO concentration (A) and NO<sub>2</sub> concentration (B) in outlet gas vs. reaction time using different catalysts under reaction conditions of light intensity = 750  $\mu\text{W cm}^{-2}$ ; humidity = 15,700 ppm; EBRT = 72



FIG.1

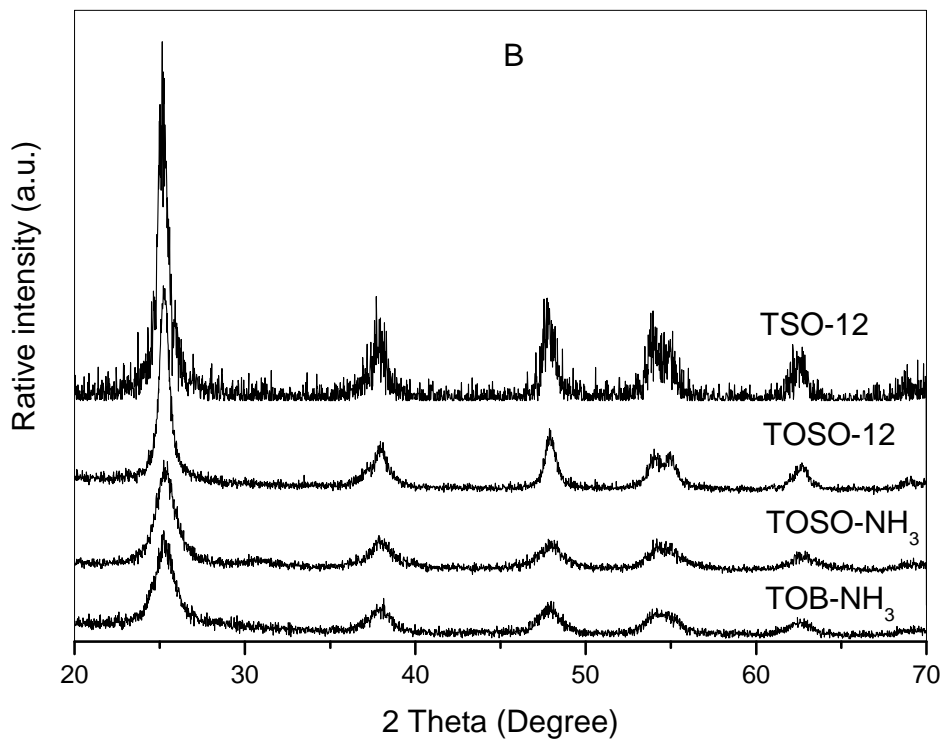
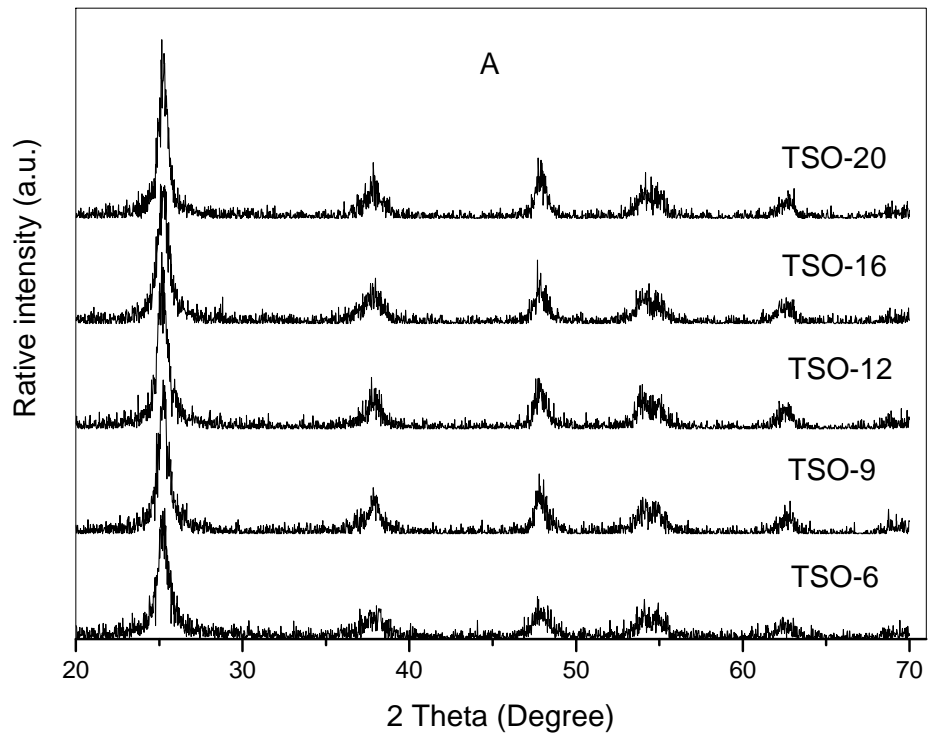


FIG.2

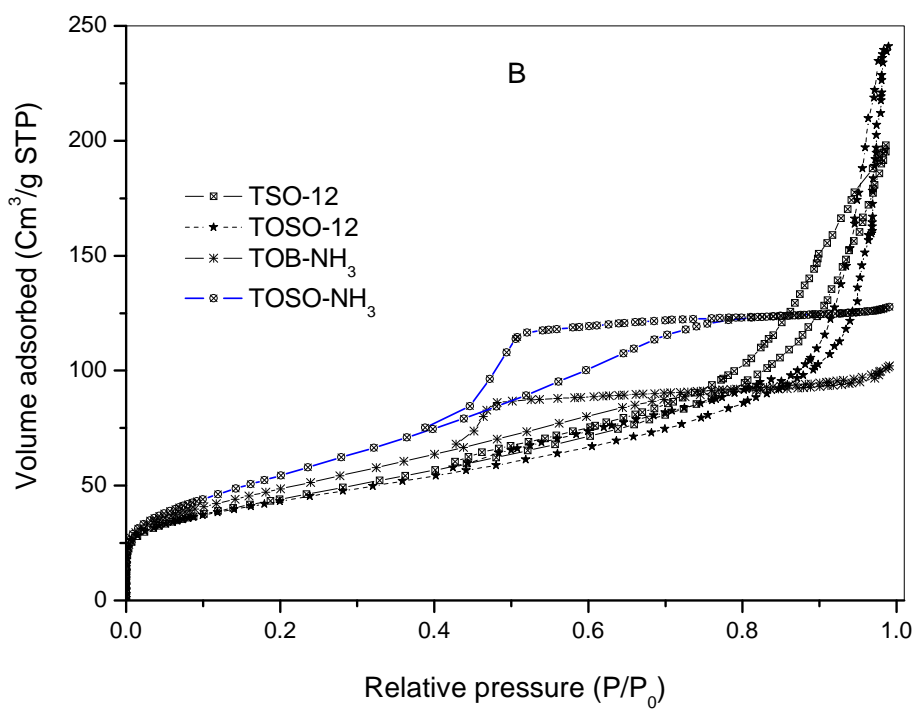
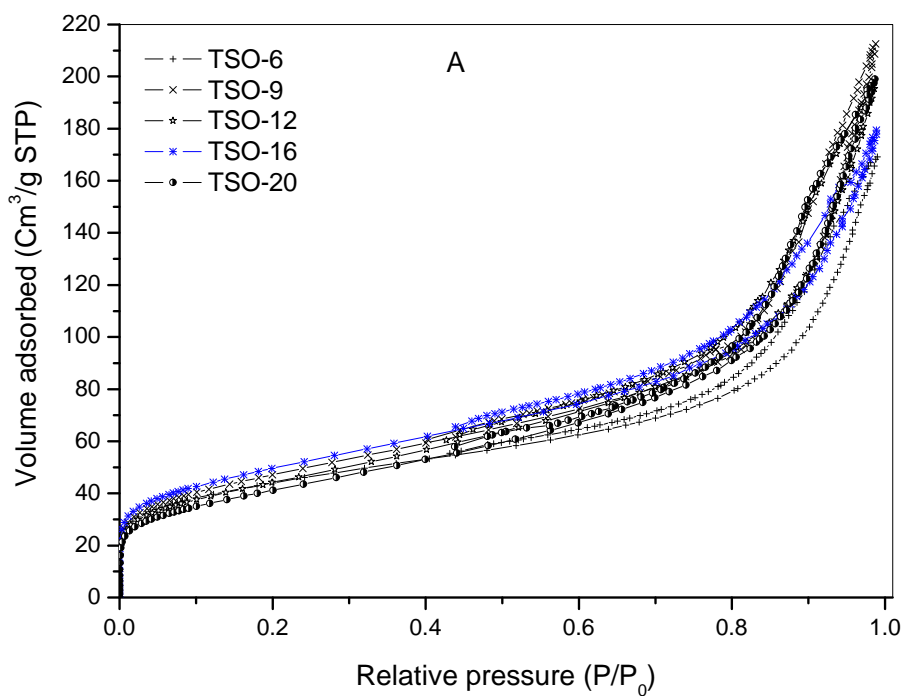


FIG.3

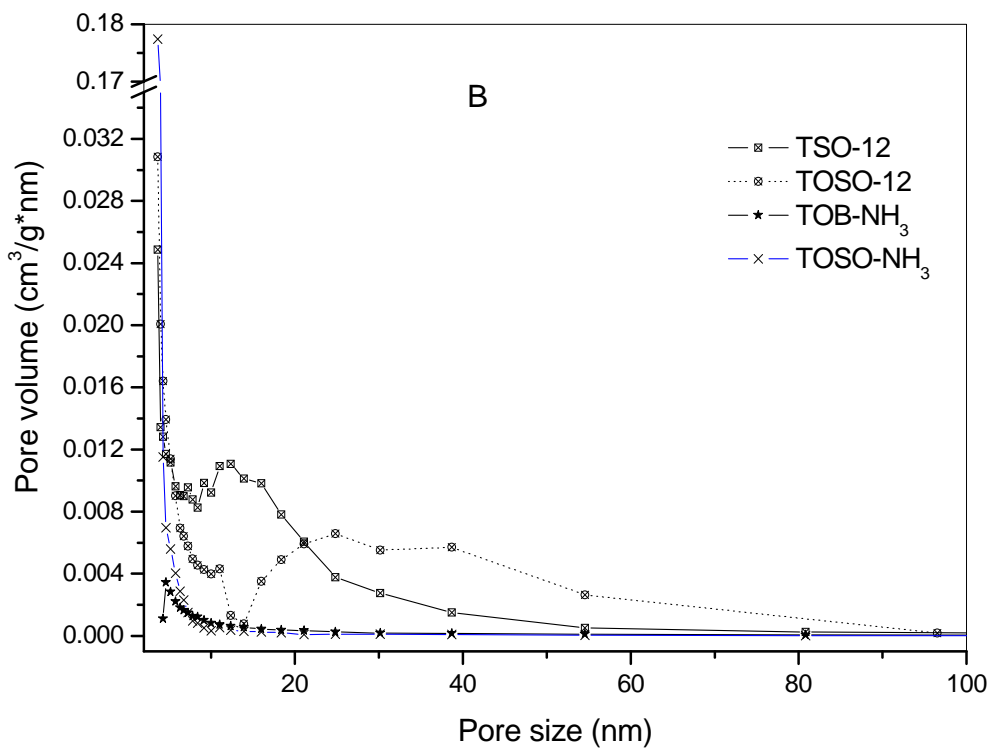
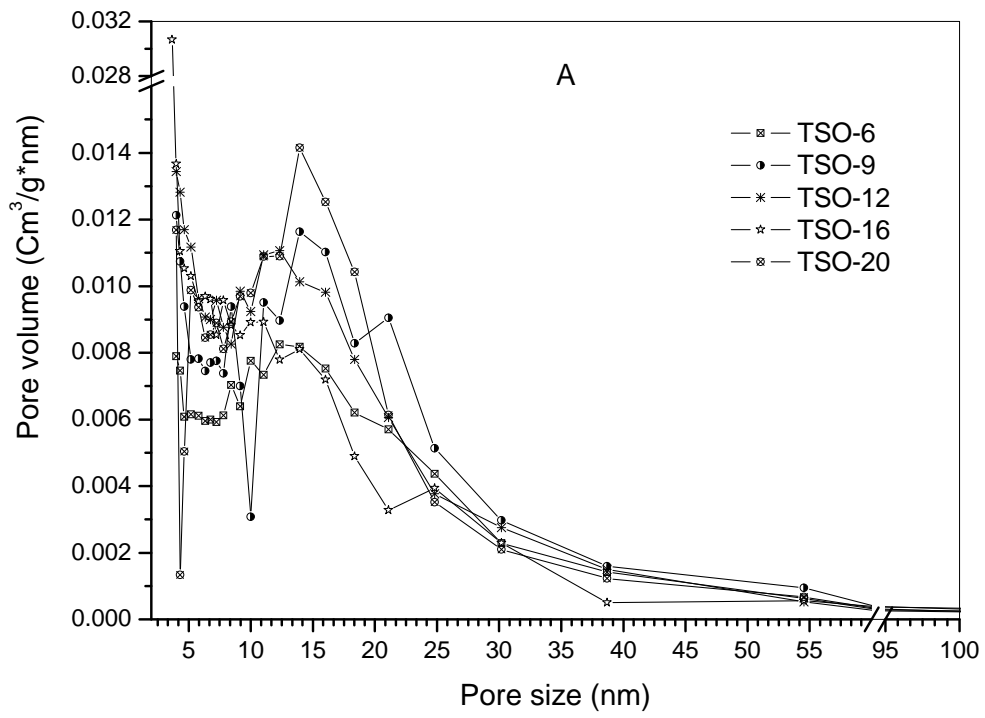


FIG. 4

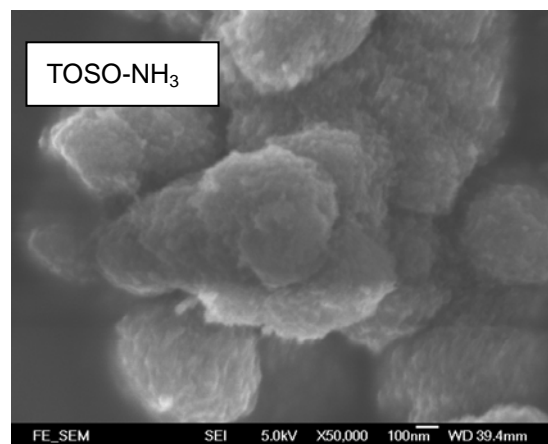
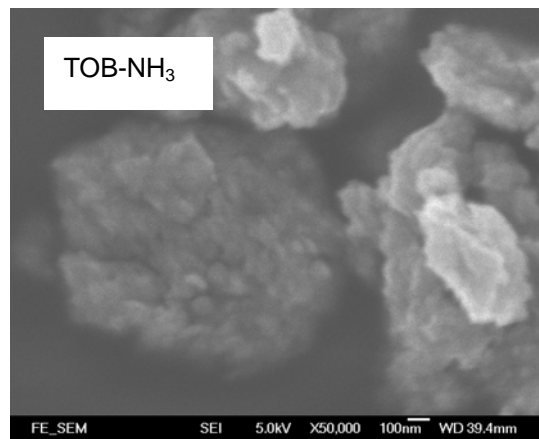
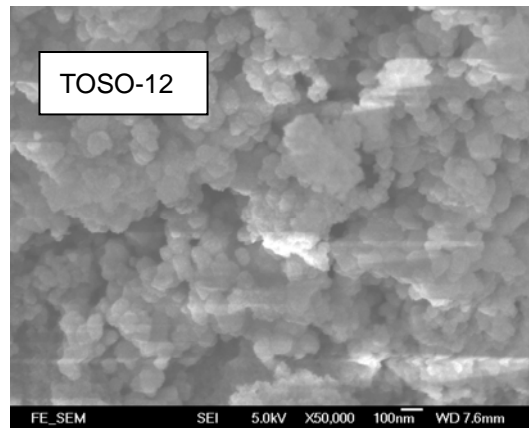
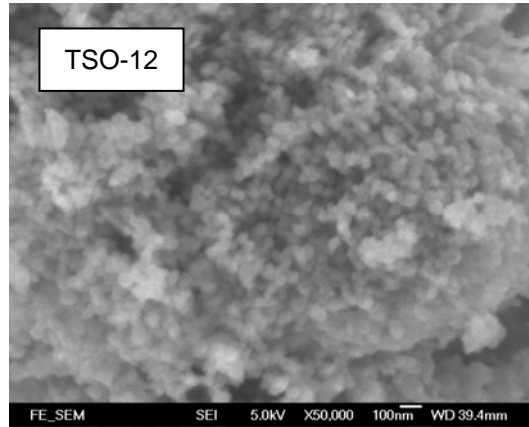


FIG. 5

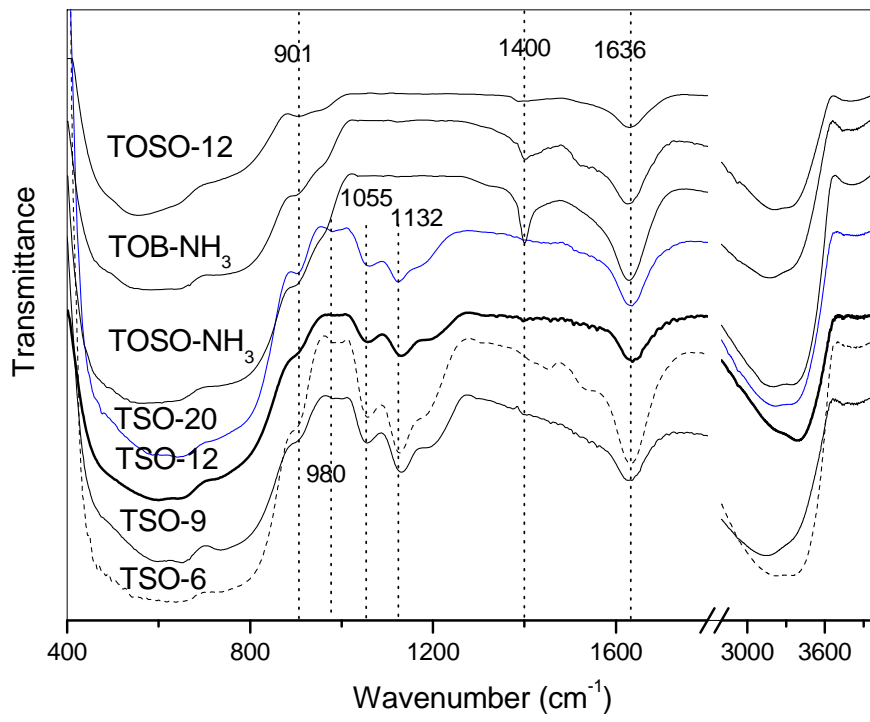


FIG. 6

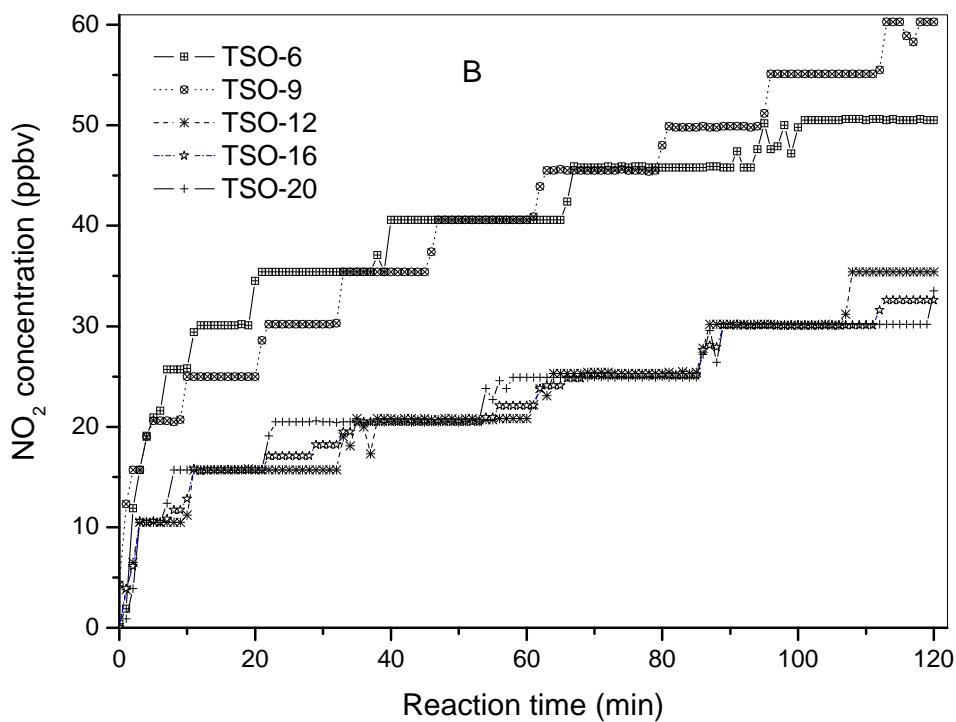
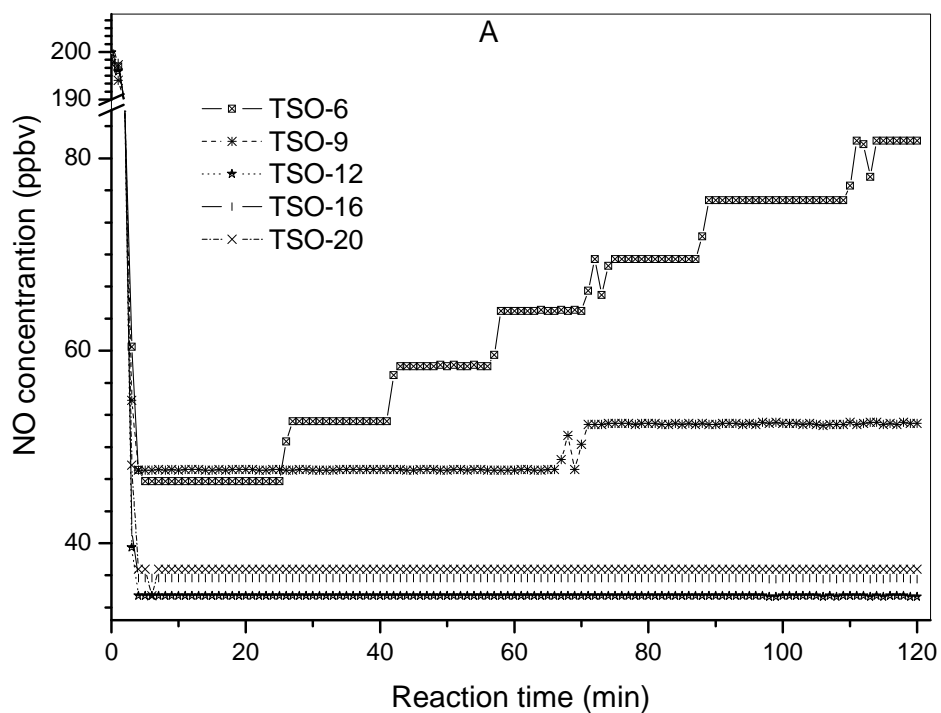


FIG. 7

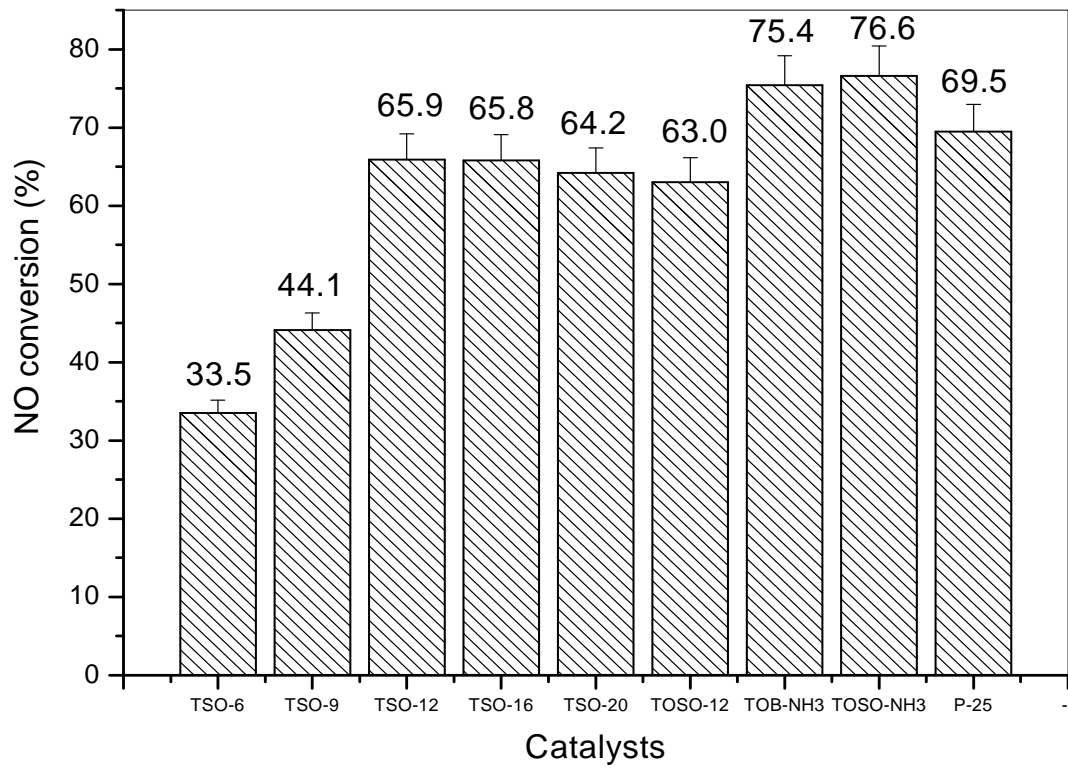


FIG. 8

